Bistatic Signal Penetration Geometry over Land Ice for the Harmony Mission

Georg Fischer [a], Kristina Belinska[b], Andreas Benedikter[a], Kostas Papathanassiou[a], Irena Hajnsek[a,c], Helmut Rott[d], Thomas Nagler[d], Pau Prats-Iraola[a]
[a] German Aerospace Center (DLR), Germany
[b] Technical University of Denmark (DTU Space), Denmark
[c] ETH Zurich, Switzerland
[d] ENVEO, Austria

Abstract

To derive elevation models and topographic change of glaciers and ice sheets, the Harmony mission's across-track InSAR phase requires accurate elevation bias correction due to signal penetration into dry snow, firn, and ice. This paper extends a monostatic penetration bias model to the bistatic geometry, incorporating the effect of the large squint angle between transmitter and receiver. The calculations show only a few percent difference in 2-way penetration depth between the bistatic Harmony geometry and conventional monostatic InSAR for identical signal extinction and penetration length. The derived bistatic volume decorrelation model establishes the relationship between coherence, phase, and penetration depth. This allows a penetration bias correction of individual Harmony interferograms, assuming constant, isotropic signal extinction, as already established for monostatic InSAR.

1 Introduction

The European Space Agency's (ESA) Harmony mission [1][2] will represent a significant advancement in the monitoring of Earth's cryosphere, with a focus on closing observation gaps of the mass balance of ice sheets and glaciers. It will consist of two passive SAR receivers flying in formation with Sentinel-1, which acts as the illuminator.
The Across-Track Interferometry (XTI) mission phase is designed to provide high-resolution topographic information over vast areas of glaciated terrain, by means of single-pass SAR interferometry (InSAR). One of the primary applications of the XTI data will be the derivation of topographic change (TOC) products, which are essential for understanding the dynamics of land ice systems.
The generation of digital surface models (DSM) of glaciers with InSAR is an established technique [3][4][5], but is affected by an elevation bias due to the penetration of the microwave signals into dry snow, firn, and ice. InSAR penetration biases at C-band frequencies from few meters down to -13 m have been measured [6][7], depending on the snow, firn, and ice conditions, as well as on polarization, incidence angle, and interferometric baseline. C-band penetration biases of down to -19 m can be inferred from signal penetration estimations from the dry snow zone in the interior of ice sheets [8][9].
Different approaches have been followed to address the bias, by using indicators of constant penetration bias [4], selected acquisitions during melting periods to minimize penetration [10], and by empirically deriving altitude-dependent bias estimates [5]. Recently, statistical and machine learning approaches, calibrated on large amounts of reference data have shown promising results [11][12][13]. The spatial and temporal differences in penetration, requirements on large training data, and the dependence of the bias on the acquisition geometry hamper these approaches for the Harmony mission.
An alternative option to account for the bias is the use of scattering models. Studies indicated the potential of a model-based estimation of the phase center depth directly from InSAR data [8][14][15][16], which is foreseen as the baseline approach for the penetration bias correction of individual interferograms of the Harmony mission.
This paper extends this monostatic penetration bias model to the bistatic acquisition geometry of Harmony. First the Harmony InSAR geometry is described and the monostatic model briefly recapped. The bistatic penetration bias model is then derived from the bistatic penetration geometry of Harmony. Model results are shown to illustrate the behavior of coherence, phase and penetration bias and to compare the monostatic and bistatic cases.

2 Harmony Across-Track InSAR

The two passive receivers Harmony A and B will have the same orbit as Sentinel-1, the active illuminator, but with an along-track separation of 350 km between Sentinel-1 and the Harmonies, see **Figure 1**. The Harmonies receive the transmitted signals, after scattering at the Earth's surface, with squint angles ψ of 26° (near range) to 20° (far range). The fundamental interferometric observable is the complex coherence γ, which describes the complex correlation between the two simultaneous, single-pass InSAR measurements s_{HA}, s_{HB} separated by a spatial baseline B, and is given by

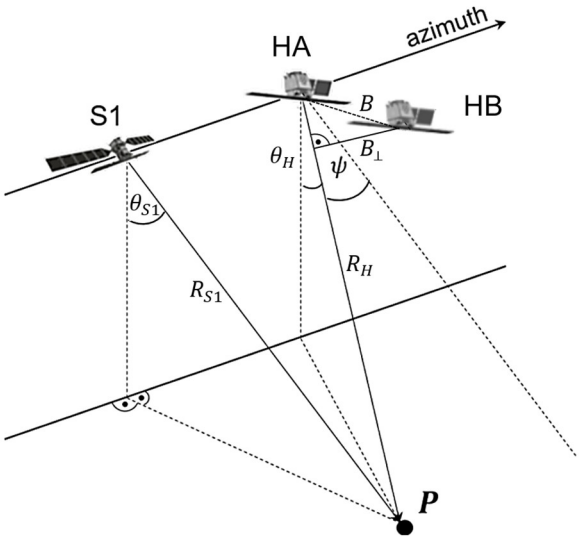

Figure 1 Harmony interferometric geometry for the XTI phase. Incidence angles θ and range distances R are shown for both Sentinel-1 (S1) and one Harmony satellite (H). The along-track separation leads to a squint angle ψ. The across-track, perpendicular baseline between Harmony A and Harmony B is $B_\perp$. Range and angles of Harmony B are omitted for clarity. Modified from [17].

$$\gamma = \frac{\langle s_{\mathrm{HA}}\, s_{\mathrm{HB}}^{*} \rangle}{\sqrt{\langle s_{\mathrm{HA}} s_{\mathrm{HA}}^{*} \rangle \langle s_{\mathrm{HB}} s_{\mathrm{HB}}^{*} \rangle}}. \tag{1}$$

The interferometric phase $\angle\gamma$ contains then information about the elevation of the scattering target on the ground and is converted to DSMs through interferometric processing [1]. On glaciers and ice sheets, the scattering phase center, and thus the derived elevation, lies below the surface, due to the microwave signal penetration in dry snow, firn and ice.

3 InSAR Penetration Bias

The penetration bias, h_b, is the difference between the scattering phase center, h_{pc}, and the true surface elevation, h_s,

$$h_b = h_{pc} - h_s. \tag{2}$$

Thus, h_b is negative with h_{pc} and h_s being positive elevation values. Assuming the interferometric phase being normalized to the surface and all other coherence terms correctly accounted for [18], the penetration bias (i.e. phase center depth) can be derived from the phase of the measured coherence γ

$$h_b = \frac{\angle\gamma}{\kappa_{zVol}} \tag{3}$$

where κ_{zVol} is the vertical wavenumber in the volume, which is described below. The depth of the scattering phase center below the surface depends on system parameters (e.g. frequency, polarization) and on the signal penetration

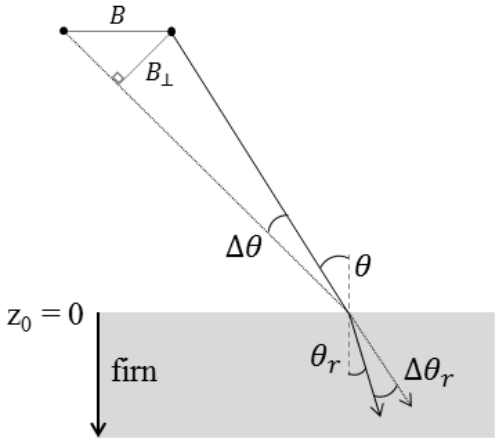

Figure 2 Across-track InSAR geometry considering the refraction into the subsurface of a glacier or an ice sheet.

due to the snow, firn, and ice conditions (e.g. wetness, grain size, scattering from ice lenses and layers). The relationship to the subsurface structure is described in terms of the volume coherence γ_{vol}.

After InSAR processing, accounting for all other coherence factors, and without temporal decorrelation, the volume coherence γ_{vol} depends on the vertical scattering profile $\sigma_v(z)$, which is the fundamental relationship for addressing the penetration bias

$$\gamma_{vol} = e^{ik_z z_0} \frac{\int_{-\infty}^{0} \sigma_v(z) e^{ik_{zVol} z} dz}{\int_{-\infty}^{0} \sigma_v(z) dz}. \tag{4}$$

The vertical scattering profile σ_v is considered a semi-infinite half space below the surface of glaciers and ice sheets. $e^{ik_z z_0}$ accounts for the interferometric phase of the surface at z_0. The general penetration and refraction geometry for across-track InSAR is depicted in **Figure 2**. κ_z is the vertical wavenumber in free space

$$\kappa_z = \frac{2\pi}{\lambda} \frac{p\, B_\perp}{R \sin\theta} = \frac{2\pi}{H_a}, \tag{5}$$

λ is the radar wavelength, R is the slant range distance, θ is the incidence angle at the air/snow interface, $B_\perp$ is the effective interferometric baseline. $p = 1$ is valid for the combination of one monostatic and one bistatic SAR image forming an interferogram, as well as for two bistatic images as in the Harmony case. $p = 2$ for the combination of two monostatic images. H_a is the height of ambiguity in free space. Accounting for the change in the propagation constant and incidence angle due to refraction [14][19][20], yields the following formulation for vertical wavenumber in the volume

$$\kappa_{zVol} = \kappa_z \sqrt{\varepsilon}\, \frac{\cos\theta}{\cos\theta_r}, \tag{6}$$

where ε is the real part of the relative dielectric permittivity and θ_r the refracted incidence angle in the volume, calculated with Snell's law.

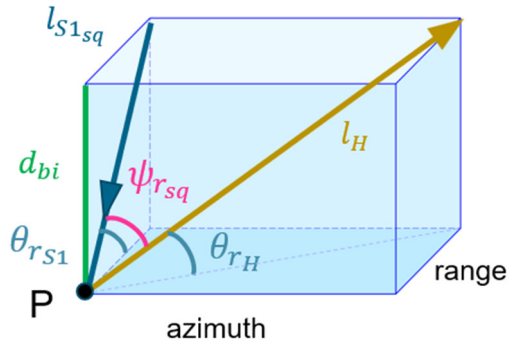

Figure 3 Sketch of the bistatic geometry with the paths and angles from Sentinel-1 ($l_{S1_{sq}}, \theta_{r_{S1}}$) to a scatterer P and from P to the Harmonies (l_H, θ_{r_H}), considering the refraction into a volume.

3.1 Monostatic Penetration Bias Model

The relationship between interferometric coherence and radar signal penetration as well as the retrieval of the penetration bias assuming a homogeneous scattering medium (uniform volume with constant signal extinction) is thoroughly described in literature for monostatic, zero-doppler acquisition geometries [8][14]. It also applies to bistatic InSAR with no significant along-track separation and negligible squint angles between the acquisitions, such as TanDEM-X.

Changing from the coherence magnitude formulation in [8] to complex coherence and expressing it in terms of the vertical wavenumber in the volume κ_{zVol} and the extinction κ_e (or one-way penetration depth d_p) gives

$$\gamma_{vol} = \frac{1}{1 + \frac{j \cos\theta_r \, \kappa_{zVol}}{2\kappa_e}} = \frac{1}{1 + \frac{j d_p \kappa_{zVol}}{2}}. \qquad (7)$$

The phase center depth, i.e., penetration bias, from such a modelled volume coherence is then calculated as in eq. (3). The advantage of such a simplified, constant extinction volume assumption is that the phase $\angle\gamma_{vol}$ can be directly inverted from the coherence magnitude $|\gamma_{vol}|$ through [14]

$$\angle\gamma_{vol} = \arctan\left(\sqrt{|\gamma_{vol}|^{-2} - 1}\right), \qquad (8)$$

which gives a penetration bias estimate by converting this phase to a depth with eq. (3).

4 Bistatic Penetration Bias

4.1 Bistatic Penetration Geometry

Since the bistatic scattering from snow, firn and ice is ongoing research with very little experimental evidence, only the geometry aspects of the bistatic Harmony acquisition geometry are considered. The same scattering properties as in the monostatic case are assumed for now.

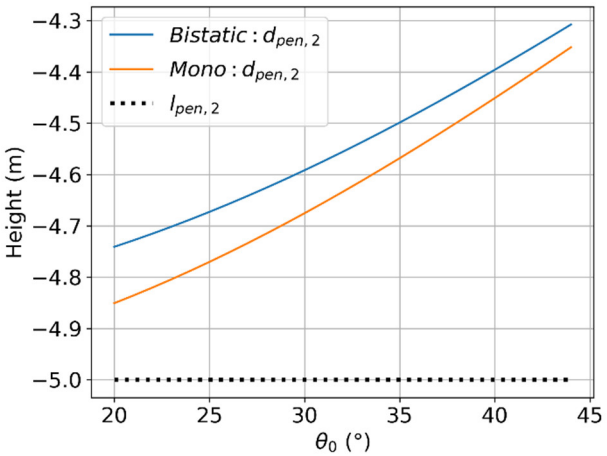

Figure 4 Bistatic and monostatic 2-way penetration *depth* for a 2-way penetration *length* of 5 m (assumed permittivity $\varepsilon = 2.0$ corresponds to a firn density of $\rho = 0.5\ g/cm^3$).

For the uniform volume model with constant extinction, the extinction is considered isotropic, thus equal for both the incident path into the volume from Sentinel-1 and the receive path towards the Harmonies.

The starting point is the understanding that, for constant isotropic extinction, the penetration *length* d_l through the volume is identical for the monostatic and bistatic geometry. **Figure 3** illustrates the bistatic penetration geometry, where the path to and from a scatterer P inside a glacier volume is $d_l = 2l_{S1}$ for the monostatic case. Instead, for the bistatic Harmony geometry, it results in

$$d_l = l_{S1_{sq}} + l_H = l_{S1_{sq}} \left(1 + \frac{1}{\cos\left(\psi_{r_{sq}}\right)}\right). \qquad (9)$$

with $\cos\psi_{r_{sq}} = \cos\theta_{H_r} / \cos\theta_{S1_r}$. The additional "sq" subscript to $l_{S1_{sq}}$ should indicate that for the squinted Harmony geometry, the path from Sentinel-1 has the same direction, but is shorter than the monostatic $d_{l_{S1}}$ for equal penetration *length* d_l. Considering length-to-depth conversion with refracted incidence angles, this leads to the derivation of a "squint factor" between the bistatic penetration depth d_{bi} and the monostatic penetration depth d_p for identical extinction (i.e. penetration length)

$$d_{bi} = f_{sq} * d_p. \qquad (10)$$

The squint factor f_{sq} is

$$f_{sq} = \frac{2}{\left(1 + \frac{1}{\cos\psi_{r_{sq}}}\right)} = \frac{2}{\left(1 + \frac{\sqrt{\varepsilon - \sin^2\theta_{S1}}}{\sqrt{\varepsilon - \sin^2\theta_H}}\right)}, \qquad (11)$$

where $\psi_{r_{sq}}$ is the refracted squint angle between the line-of-sights of Sentinel-1 and Harmony inside the volume. It can be also expressed in terms of permittivity ε and the incidence angle of Sentinel-1 θ_{S1} and the incidence angle (i.e. zenith scattering angle) of Harmony θ_H.

Figure 4 shows the resulting difference between monostatic and bistatic 2-way penetration *depths* for a common

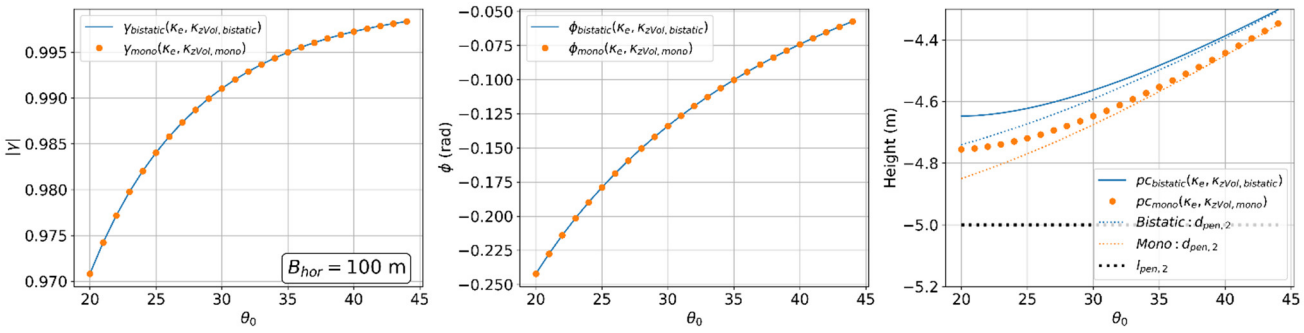

Figure 5 Coherence magnitude (left), phase (middle) and phase center depth (right) for a bistatic and monostatic geometry over Sentinel-1 incidence angle assuming an equal 2-way penetration *length* of 5 m for both monostatic and bistatic cases. The sensitivity to extinction and penetration length is equal, hence the vertical wavenumbers differ accordingly. The horizontal baseline of 100 m leads to $0.05 < \kappa_{zVol} < 0.013$ assuming $\varepsilon = 2.0$.

2-way penetration *length* of 5 m, over Sentinel-1 incidence angles. The bistatic 2-way penetration depth is slightly smaller (i.e. shallower) than its monostatic equivalent for identical extinction and penetration length. Interestingly, this difference is less than 5% for the Harmony geometry.

4.2 Bistatic Vertical Wavenumber

The calculation of the bistatic phase-to-height sensitivity is thoroughly elaborated in [21]. Assuming parallel velocity vectors for all three satellites and a flat Earth geometry, the following, much simpler, calculation for the bistatic $\kappa_{z_{bi}}$ holds

$$\kappa_{z_{bi}} = \frac{2\pi}{\lambda}\cos\psi\frac{\Delta\theta}{\sin\theta_{S1}} = \frac{2\pi}{\lambda}\frac{B_\perp}{R_H\sin\theta_{S1}}, \tag{12}$$

$\Delta\theta = B_\perp/R_{S1}$ is the difference in look angles of the two Harmonies in the across-track plane, which equals the ratio of the across-track, perpendicular baseline $B_\perp$ component of the baseline between the two Harmony satellites (**Figure 1**) and the Sentinel-1 range R_{S1}. ψ is the squint angle between the line of sights of Sentinel-1 and Harmony. For a flat earth geometry, this can be further simplified using the Harmony range distance $R_H = R_{S1}/\cos\psi$. An important step in this simple solution comes from the fact that the interferometric phase dependence on height is derived from the sensitivity to the elevation direction, which is orthogonal to the range and Doppler directions, i.e., it is the same elevation direction for Harmony XTI as for an equivalent Sentinel-1 zero-Doppler interferometer.

The conversion from free-space vertical wavenumber $\kappa_{z_{bi}}$ to vertical wavenumber in the volume $\kappa_{zVol_{bi}}$ is similar for Harmony as in the monostatic equation in (6) using the free-space θ_{S1} and refracted incidence angle $\theta_{R_{S1}}$ of Sentinel-1. Also, the refracted squint angle $\psi_{r_{sq}}$ has to be considered.

$$k_{zVol_{bi}} = k_{z_{bi}}\sqrt{\epsilon}\frac{\cos\psi_{r_{sq}}}{\cos\psi}\frac{\cos\theta_{S1}}{\cos\theta_{S1_r}}. \tag{13}$$

This solution is used in the following simulations.

4.3 Bistatic Volume Decorrelation Model

The bistatic model of the volume decorrelation $\gamma_{vol_{bi}}$ for a uniform volume has to consider the squint factor f_{sq} when using extinction or penetration length to accommodate the correct relationship to the vertical dimension of $\kappa_{zVol_{bi}}$. Alternatively, it can be also expressed in terms of the bistatic penetration depth d_{bi}, without squint factor,

$$\gamma_{vol_{bi}} = \frac{1}{1+\frac{j\cos\theta_{r_{S1}}f_{sq}\kappa_{zVol_{bi}}}{2\kappa_e}} = \frac{1}{1+\frac{jd_{bi}\kappa_{zVol_{bi}}}{2}}. \tag{14}$$

Figure 5 illustrates the coherence, phase and penetration depth of a monostatic zero-Doppler interferogram and a bistatic Harmony interferogram, assuming a common 2-way penetration length of 5 m and enforcing equal interferometric sensitivity to penetration *length*. This means, the mono- and bistatic vertical wavenumbers are adjusted in way that results in the same interferometric phase for the same path length in the volume for both cases. This equal sensitivity to penetration length leads to a difference between the vertical wavenumbers of factor f_{sq}.

This comparison illustrates the understanding that monostatic and bistatic coherence (**Figure 5**, left) and phase (**Figure 5**, middle) are identical w.r.t extinction or penetration length, but differ w.r.t penetration depth (**Figure 5**, right), for the case of common penetration length and common interferometric sensitivity to penetration length. Then, coherence and phase are equal and the difference is only in the conversion to depth. For the Harmony geometry, the bistatic penetration depth is less than 5% smaller than the monostatic penetration depth for free-space propagation. The difference is even less for $\varepsilon > 1$. **Figure 5** right shows a deviation between two-way penetration depths (thin dotted lines, also shown in **Figure 4**) and phase center depths (i.e. penetration bias) at smaller incidence angles, which is a known effect for increasing perpendicular baselines [14][15].

The above model formulation holds for the case of constant, isotropic signal extinction, based on the interferometric decorrelation along the propagation path through the volume, which leads to the described differences in penetration depth between mono- and bistatic scenarios.

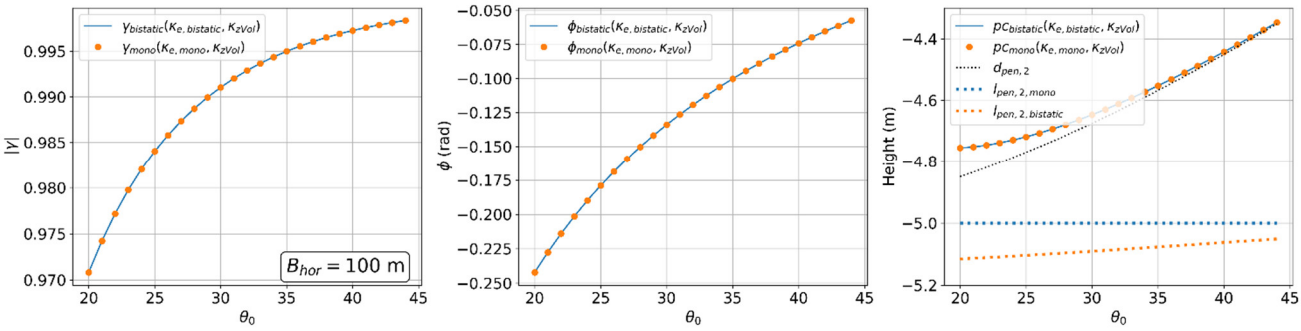

Figure 6 Coherence magnitude (left), phase (middle) and phase center depth (right) for a bistatic and monostatic geometry over Sentinel-1 incidence angle assuming equal 2-way penetration *depth* and equal vertical wavenumbers for both monostatic and bistatic cases. All values are equal to the monostatic case of **Figure 5**, except for the bistatic penetration *length,* which has to be larger in order to have equal penetration *depth*.

However, this should not be confused with the general volume decorrelation relationship, which is based on the real physical depth of scattering contributions $\sigma_v(z)$. Here, the relationship stays the same as in (4) except for the difference in the calculation of the vertical wavenumber.

$$\gamma_{vol_{bi}} = e^{ik_z z_0} \frac{\int_{-\infty}^{0} \sigma_v(z) e^{ik_{zVol_{bi}} z} dz}{\int_{-\infty}^{0} \sigma_v(z) dz} \tag{15}$$

Assuming an identical vertical scattering profile and identical vertical wavenumbers for a monostatic and bistatic interferometric geometry, would lead to the same coherence and phase, but the bistatic signals would then experience a longer propagation path in the volume (larger penetration *length*, smaller extinction). This is illustrated in **Figure 6**, where penetration depth and vertical wavenumber are equal for both mono- and bistatic, but this requires a larger bistatic penetration length (**Figure 6**, right). This is different to the idea illustrated in **Figure 5**, where the interferometric sensitivity to extinction and penetration length is identical, but with the resulting difference in vertical wavenumber and penetration depth.

5 Conclusion and Outlook

The Harmony mission will produce InSAR elevation measurements of glaciers and ice sheets that are affected by the elevation bias due to signal penetration. This paper demonstrates how the effect of the bistatic geometry, with significant squint angles between transmitter and receiver, on this penetration bias can be accounted for. It follows that the established uniform volume model inversion of the coherence magnitude [14][15][16], cf. eq. (8), can be equally applied to the bistatic Harmony geometry to estimate the penetration bias on individual interferograms. Only the conversion to depth differs as shown. In fact, it is planned that the penetration bias will be corrected in terms of its phase, during the generation of the DSM. Range shifts will be accounted for accordingly [22].

So far, this was derived under the assumption of constant, isotropic signal extinction. Future work will address the impact of non-isotropic extinction by considering effects of bistatic scattering from snow, firn and ice. Due to the lack of experimental data at such bistatic angles, the investigations will be conducted through modelling of the canonical scattering elements.

6 Literature

[1] European Space Agency, "Report for Mission Selection: Earth Explorer 10 Candidate Mission Harmony," ESA-EOPSM-HARM-RP-4129, European Space Agency, Noordwijk, The Netherlands, Jun. 2022.

[2] A. Kääb et al., "Potential of the Bi-Static SAR Satellite Companion Mission Harmony for Land-Ice Observations," Remote Sensing, vol. 16, no. 16, p. 2918, Aug. 2024, doi: 10.3390/rs16162918.

[3] M. Zemp et al., "Global glacier mass changes and their contributions to sea-level rise from 1961 to 2016," Nature, vol. 568, no. 7752, pp. 382–386, Apr. 2019, doi: 10.1038/s41586-019-1071-0.

[4] H. Rott et al., "Changing pattern of ice flow and mass balance for glaciers discharging into the Larsen A and B embayments, Antarctic Peninsula, 2011 to 2016," The Cryosphere, vol. 12, no. 4, Art. no. 4, Apr. 2018, doi: 10.5194/tc-12-1273-2018.

[5] J. Gardelle, E. Berthier, Y. Arnaud, and A. Kääb, "Region-wide glacier mass balances over the Pamir-Karakoram-Himalaya during 1999-2011," The Cryosphere, vol. 7, no. 4, pp. 1263–1286, Aug. 2013.

[6] J. Dall, S. N. Madsen, K. Keller, and R. Forsberg, "Topography and penetration of the Greenland Ice Sheet measured with Airborne SAR Interferometry," Geophysical Research Letters, vol. 28, no. 9, Art. no. 9, May 2001, doi: 10.1029/2000GL011787.

[7] E. Rignot, K. Echelmeyer, and W. Krabill, "Penetration depth of interferometric synthetic-aperture radar signals in snow and ice," Geophysical Research Letters, vol. 28, no. 18, Art. no. 18, Sept. 2001, doi: 10.1029/2000GL012484.

[8] E. Weber Hoen and H. A. Zebker, "Penetration depths inferred from interferometric volume decorrelation observed over the Greenland Ice Sheet," IEEE Trans. Geosci. Remote Sensing, vol. 38, no. 6, Art. no. 6, Nov. 2000, doi: 10.1109/36.885204.

[9] H. Rott, K. Sturm, and H. Miller, “Active and passive microwave signatures of Antarctic firn by means of field measurements and satellite data,” Ann. Glaciol., vol. 17, pp. 337–343, 1993, doi: 10.3189/S0260305500013070.

[10] W. Abdel Jaber, H. Rott, D. Floricioiu, J. Wuite, and N. Miranda, “Heterogeneous spatial and temporal pattern of surface elevation change and mass balance of the Patagonian ice fields between 2000 and 2016,” The Cryosphere, vol. 13, no. 9, pp. 2511–2535, Sept. 2019, doi: 10.5194/tc-13-2511-2019.

[11] S. Abdullahi, D. Burgess, B. Wessel, L. Copland, and A. Roth, “Quantifying the impact of X-band InSAR penetration bias on elevation change and mass balance estimation,” Ann. Glaciol., pp. 1–15, Feb. 2024, doi: 10.1017/aog.2024.7.

[12] A. B. Campos, A. Diez-Latteur, J-L. Bueso-Bello, M. Braun and P. Rizzoli, "A Snow Properties-Aware Deep Learning Framework for Penetration Bias Estimation of Tandem-X DEMs over Ice Sheets," Remote Sensing of Environment, submitted, 2025.

[13] I. Mansour, G. Fischer, R. Hänsch, and I. Hajnsek, “Hybrid AI-Physical Modeling for Penetration Bias Correction in X-band InSAR DEMs: A Greenland Case Study,” in Proceedings of the Computer Vision and Pattern Recognition Conference (CVPR) Workshops, June 2025, pp. 2209–2218.

[14] J. Dall, “InSAR Elevation Bias Caused by Penetration Into Uniform Volumes,” IEEE Trans. Geosci. Remote Sensing, vol. 45, no. 7, 2007.

[15] G. Fischer, K. P. Papathanassiou, and I. Hajnsek, “Modeling and Compensation of the Penetration Bias in InSAR DEMs of Ice Sheets at Different Frequencies,” IEEE J. Sel. Top. Appl. Earth Observations Remote Sensing, vol. 13, 2020.

[16] H. Rott et al., “Penetration of interferometric radar signals in Antarctic snow,” The Cryosphere, vol. 15, no. 9, Art. no. 9, Sept. 2021, doi: 10.5194/tc-15-4399-2021.

[17] A. Benedikter et al., “Toward Dry Snow Parameter Estimation by Simultaneous Multiple Squint Differential InSAR,” IEEE Trans. Geosci. Remote Sensing, vol. 62, pp. 1–15, 2024, doi: 10.1109/TGRS.2024.3486328.

[18] H. A. Zebker and J. Villasenor, “Decorrelation in interferometric radar echoes,” IEEE Trans. Geosci. Remote Sensing, vol. 30, no. 5, Art. no. 5, Sept. 1992, doi: 10.1109/36.175330.

[19] J. J. Sharma, I. Hajnsek, K. P. Papathanassiou, and A. Moreira, “Estimation of Glacier Ice Extinction Using Long-Wavelength Airborne Pol-InSAR,” IEEE Trans. Geosci. Remote Sensing, vol. 51, no. 6, 2013.

[20] Y. Lei, P. Siqueira, and R. Treuhaft, “A dense medium electromagnetic scattering model for the InSAR correlation of snow,” Radio Science, vol. 51, no. 5, pp. 461–480, May 2016, doi: 10.1002/2015RS005926.

[21] A. Theodosiou and P. López-Dekker, “On the Sensitivity to Height and Motion of Bistatic SAR Interferometry: A Spectral View,” IEEE Trans. Geosci. Remote Sensing, vol. 62, pp. 1–12, 2024, doi: 10.1109/TGRS.2024.3399598.

[22] A. Benedikter, M. Rodriguez-Cassola, P. Prats-Iraola, G. Krieger, and G. Fischer, “On the Processing of Single-Pass InSAR Data for Accurate Elevation Measurements of Ice Sheets and Glaciers,” IEEE Trans. Geosci. Remote Sensing, vol. 62, pp. 1–10, 2024, doi: 10.1109/TGRS.2023.3345415.